

Clustering-based multi-view network fusion for estimating brain network atlases of healthy and disordered populations

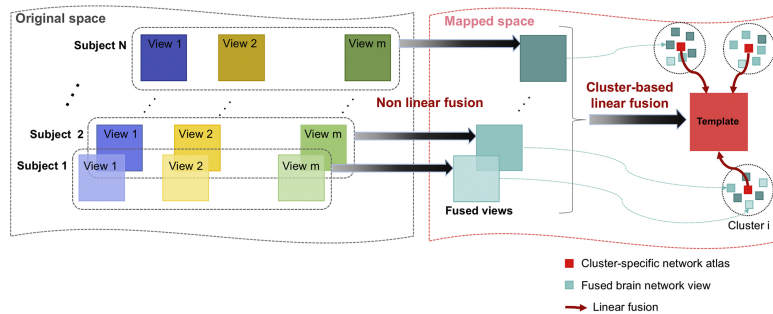


Salma Dhifallah^{a,b}, Islem Rekik^{a,*}, for the Alzheimer's Disease Neuroimaging Initiative¹

^a BASIRA Lab, CVIP Group, School of Science and Engineering, Computing, University of Dundee, UK

^b Computer Engineering Department Ecole Nationale d'ingénieurs de Sousse Sousse Tunisia

GRAPHICAL ABSTRACT



ARTICLE INFO

Keywords:

Multi-view brain networks
Brain morphology
Network atlas
Network fusion
T1-w MRI

ABSTRACT

Background: While several research methods were developed to estimate *individual-based* representations of brain connective wiring (i.e., a connectome), traditionally captured using multimodal MRI data (e.g., functional and diffusion MRI), very limited works aimed to estimate *brain network atlas* for a *population* of connectomes. Estimating well-representative brain templates is a key step for group comparison studies. However, estimating a network atlas for a population of multi-source brain connectomes lying on different manifolds is absent.

New method: To fill this gap, we propose a cluster-based multi-view brain connectivity fusion framework to estimate a brain network atlas for a population of multi-view brain networks, where each view captures a specific facet of the brain construct. Specifically, given a population of subjects, each with multi-view networks, we first non-linearly fuse multi-view networks into a single fused network for each subject. Then, we cluster the fused networks to identify individuals sharing similar connective traits in an unsupervised way, which are next averaged within each cluster to generate a representative network atlas. Finally, we construct the final multi-view network atlas by averaging the obtained templates of all clusters.

Results: We evaluated our method on both healthy and disordered populations (with autism and dementia) and spotted differences between network atlases for healthy and autistic groups.

Comparison with existing methods and conclusions: Compared to other baseline methods, our fusion strategy achieved the best results in terms of template centeredness and population representativeness.

* Corresponding author.

E-mail address: irekik@dundee.ac.uk (I. Rekik).

¹ Data used in preparation of this article were obtained from the Alzheimer's Disease Neuroimaging Initiative (ADNI) database (adni.loni.usc.edu). As such, the investigators within the ADNI contributed to the design and implementation of ADNI and/or provided data but did not participate in analysis or writing of this report. A complete listing of ADNI investigators can be found at: http://adni.loni.usc.edu/wp-content/uploads/how_to_apply/ADNI_Acknowledgement_List.pdf

<https://doi.org/10.1016/j.jneumeth.2018.09.028>

Received 1 August 2018; Received in revised form 11 September 2018; Accepted 25 September 2018

Available online 30 September 2018

0165-0270/ © 2018 Elsevier B.V. All rights reserved.

1. Introduction

The study of brain connections has been widely developed for the last years (Brown and Hamarneh, 2016; Holmes et al., 2015) thanks to the wealth of connectomic data collected through several projects including Human Connectome Project (HCP) (Van Essen et al., 2012, 2013), Lifespan Baby Connectomes Project (BCP) (Van Essen and Glasser, 2016), and Connectome Related to Human Disease (CRHD) (Van Essen and Glasser, 2016). Therefore, connectomic data estimated from structural (T1-w/T2-w), diffusion-weighted (DWI) and resting-state functional (rsfMRI) magnetic resonance imaging (MRI) modalities is rapidly expanding (Lerch et al., 2017). The richness of these multimodal connectomic brain data can offer a powerful tool for better understanding of the human brain construct (Sporns, 2012, 2013), as well as capturing disordered brain alterations, (Bosc et al., 2003; Iftekharuddin et al., 2009; Calhoun and Sui, 2016). However, the analysis of multimodal brain networks, which captures different views of the brain construct, is a relatively complicated task (Bullmore and Sporns, 2009; Bullmore and Bassett, 2011). Data fusion and concatenation techniques have been widely used to comprehensively integrate individual-based brain network from multiple brain views, where each brain view corresponds to an imaging modality or a unique connectomic representation of the brain (Sui et al., 2012). For instance, Wee et al. (2012), introduced a multiple-kernel support vector machines to integrate information from structural and functional networks for mild cognitive impairment diagnosis. In recent works (Lisowska et al., 2017; Soussia and Rekik, 2017; Mahjoub et al., 2018), morphological brain networks quantifying dissimilarities between cortical regions were concatenated for dementia and autism diagnosis. However, to the best of our knowledge, existing methods focus on fusing multimodal connectomic information at the individual level – and not the population level.

Recently, Rekik et al. (2017) introduced the concept of a brain network atlas (or network atlas), and proposed diffusive-shrinking graph technique to estimate a centered network atlas using a set of unimodal brain networks. However, this work was limited to investigating unimodal networks, encoding a single ‘view of the brain’. Creating such a multimodal brain network atlas can leverage and integrate complementary aspects of multimodal connections derived from diverse imaging modalities (Uludağ and Roebroeck, 2014), since each modality offers limited and complementary information apart. In addition, defining a ‘normalization’ process of brain networks can reduce inter-subject variability (Uyilings et al., 2005) offering a tool to distinguish between healthy and disordered population to help better identify ‘pathological’ alterations in brain networks as deviations from the ‘normalized’ brain network representation (Hinrichs et al., 2011; Zhang et al., 2011; Yuan et al., 2012; Thung et al., 2014; Tong et al., 2015). To fill this gap, we propose a cluster-based multi-view brain connectivity fusion framework to estimate a brain network atlas for a population of multi-view brain networks, which satisfies the following constraints: 1) it is well centered (i.e., occupying a center position near to all views and all individuals), and 2) it is well-representative of a specific population as it preserves shared traits across its individuals. Specifically, given a population of subjects, each with multi-view networks where each modality captures a brain connectomic view, we first non-linearly fuse multi-view networks into a single fused network for each individual. Then, we cluster the fused networks to identify individuals sharing similar connectomic traits in an unsupervised way. Next, through averaging networks in each cluster, we generate a representative network atlas. Finally, we construct the final multi-view network atlas by averaging the obtained representations of all clusters. Using our proposed method, we compare multi-view network atlases estimated using a healthy population (normal controls – NC) and a disordered population diagnosed with Autism Spectrum Disorder (ASD).

Table 1

Major mathematical notations used in this paper.

Mathematical notation	Definition
N	Total number of subjects in the population
n	Number of regions of interest (ROIs)
m	Total number of brain views for each subject
\mathbf{V}_k^v	v th brain network view for subject k
\mathbf{F}_k	Fused views for subject k
\mathbf{P}_k^v	Status matrix for view v and subject k
\mathbf{S}_k^v	Kernel matrix for view v and subject k
N_i	Set of neighbours for ROI i using KNN algorithm
q	Number of neighbours used for KNN algorithm
N_t	Number of iterations in SNF
N_c	Number of clusters
\mathbf{F}^{C_i}	Cluster-specific network atlas for cluster C_i
\mathbf{A}	Final estimated network atlas

KNN, K nearest neighbors; SNF, similarity network fusion.

2. Proposed method

In this section, we denote tensors by boldface Euler script letters, e.g., \mathbf{X} . Matrices are denoted by boldface capital letters, e.g., \mathbf{X} , and scalars are denoted by lowercase letters, e.g., x . For easy reference and enhancing the readability, we have summarized the major mathematical notations in Table 1.

In this section, we detail each step of our proposed cluster-based multi-view brain connectivity fusion framework to estimate a brain network atlas for a population of multi-view brain networks. First, we model each unimodal brain network as a complete graph comprising n nodes, where each node denotes an anatomical region of interest (ROI) in the brain and the strength of each edge connecting two ROIs captures their relationship in a particular aspect (e.g., brain function or morphology). This can be mathematically defined as an $n \times n$ symmetric connectivity matrix \mathbf{V} , where each element $v_{ij} \in \mathbf{V}$ denotes the connectivity weight between two ROIs i and j . A single brain connectivity between two ROIs can be measured using different MRI modalities. If one looks at each modality (e.g., rsfMRI) as capturing a single ‘view’ of the brain, then multiple brain imaging modalities can be leveraged to produce a *multi-view representation of the brain*. Hence, to develop an *effective network fusion method* for constructing a multi-view brain network atlas, one needs to well capture these multi-view (or multi-view) connectomic aspects.

Given a population of N subjects, each subject k is represented by a set of m different brain network views $\{\mathbf{V}_k^1, \mathbf{V}_k^2, \dots, \mathbf{V}_k^m\}$. Our goal is to estimate a multi-view network atlas that is well-centered (close to all views \mathbf{V}_k^v and all N subjects) and preserves shared multi-view connectomic trends across individuals. Fig. 1 shows the three main steps of the proposed method.

Individual-based non-linear fusion of connectomic brain views (step 1). For each subject in the population, different views of brain network might lie on different multi-view manifolds. A non-linear fusion function ϕ is then needed in order to derive a unique representative matrix \mathbf{F}_k for the m views as follows:

$$\phi(\{\mathbf{V}_k^v\}_{v=1}^m) \mapsto \mathbf{F}_k \quad (1)$$

Basically, for each subject k , ϕ non-linearly maps the multi-view networks $\{\mathbf{V}_k^v\}_{v=1}^m$ to a fused brain network \mathbf{F}_k in the mapped or ‘fusion’ space. This allows to map all individuals to a common space where their brain views are unified individually. To do so, we leverage the generic similarity network fusion (SNF) developed by Wang et al. proposed in Wang et al. (2014). Specifically, we use SNF to define our mapping function ϕ in order to diffuse multi-view brain networks from the original space into the mapped space where they are fused. Given a subject k , for each connectivity matrix \mathbf{V}_k^v , $v \in \{1, \dots, m\}$, we define a status

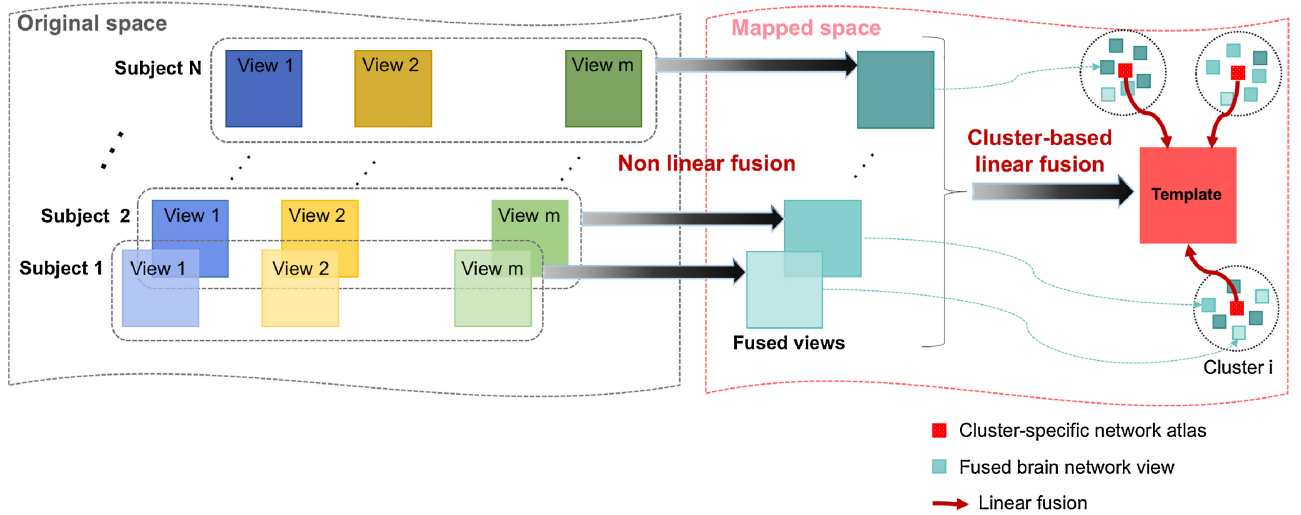


Fig. 1. Illustration of the proposed multi-view brain network atlas estimation. Given a population of N subjects, each individual has m brain connectional views (or modalities). We first non-linearly fuse multi-view brain network views for each subject through graph-diffusion in the original space. Second, we cluster the fused views in the mapped space into N_c clusters and produce a cluster-specific network atlas through linear fusion. Third, we estimate the final brain network atlas by averaging the N_c cluster-specific templates.

matrix \mathbf{P}_k^v that carries the full information about the connectivity weight of each pair of ROIs and a kernel matrix \mathbf{S}_k^v that encodes the similarity to the nearest ROIs for each ROI. These matrices are initially defined as follows based on Wang et al. (2014):

$$\mathbf{P}_k^v(i, j) = \begin{cases} \frac{\mathbf{V}_k^v(i, j)}{2 \sum_{l \neq i} \mathbf{V}_k^v(i, l)} & j \neq i \\ 1/2, & j = i \end{cases} \quad (2)$$

$$\mathbf{S}_k^v(i, j) = \begin{cases} \frac{\mathbf{V}_k^v(i, j)}{\sum_{l \in N_i} \mathbf{V}_k^v(i, l)} & j \in N_i \\ 0, & \text{otherwise} \end{cases} \quad (3)$$

N_i represents the set of q neighbors of ROI i using KNN algorithm. In order to integrate the different views into a single matrix, the status matrices \mathbf{P}_k^v are iteratively updated using this equation:

$$\mathbf{P}_k^v = \mathbf{S}_k^v \times \left(\frac{\sum_{t \neq v} \mathbf{P}_k^t}{m-1} \right) \times (\mathbf{S}_k^v)^T, \quad v \in \{1, \dots, m\} \quad (4)$$

For each subject k and view v , \mathbf{P}_k^v is iteratively updated through diffusing the global structure of other views $\left(\frac{\sum_{t \neq v} \mathbf{P}_k^t}{m-1} \right)$ along the local sparse structure \mathbf{S}_k^v of the current view v . After N_t iterations, we obtain the fused views of subject k by averaging (i.e., fusing) the diffused status matrices \mathbf{P}_k^v at the final iteration N_t :

$$\mathbf{F}_k = \frac{\sum_{v=1}^m \mathbf{P}_k^v}{m} \quad (5)$$

The update of \mathbf{P}_k^v allows to iteratively integrate common as well as complementary information across brain networks during the fusion process.

Fused network clustering in the mapped (fusion) space (step 2). During non-linear fusion using SNF, weak connections within multi-view networks disappear and strong connections are added to one another. Therefore, network heterogeneous distribution present in the original space might persist in the mapped space. Hence, instead of directly fusing heterogeneous data samples in one step, we adopt a hierarchical merging step where we first identify individuals sharing similar connectional traits, then group them into more homogenous clusters in an unsupervised way. In this step, we use spectral clustering technique to cluster the fused networks $\{\mathbf{F}_k\}_{k=1}^N$ in the mapped space into N_c clusters. Spectral clustering is an effective tool for capturing global structure of graphs, so we start by constructing a similarity network

between the fused views \mathbf{F}_k , where the strength of each connection between two fused networks \mathbf{F}_i and \mathbf{F}_j is defined as the distance between the vectorized upper triangular parts of both matrices (as they are symmetric). Spectral clustering is then applied to obtain the final partition label vector \mathbf{y} , where y_i denotes the label of the cluster to which the network \mathbf{F}_i belongs. This produces N_c cluster-specific network atlases for each cluster C_i as follows:

$$\mathbf{F}^{C_i} = \frac{\sum_{k \in C_i} \mathbf{F}_k}{\dim(C_i)} \quad (6)$$

where $\dim(C_i)$ denotes the number of elements in cluster C_i .

Linear fusion (step 3). After obtaining the cluster-based brain templates $\{\mathbf{F}^{C_i}\}_{i=1}^{N_c}$, we linearly average them into a single template denoting our multi-view network atlas \mathbf{A} as follows:

$$\mathbf{A} = \frac{\sum_{i=1}^{N_c} \mathbf{F}^{C_i}}{N_c} \quad (7)$$

3. Results and discussion

Evaluation dataset and parameters. We evaluated the proposed network atlas estimation framework on 341 subjects (155 ASD and 186 NC) from Autism Brain Imaging Data Exchange (ABIDE I)² public dataset, in addition to 41 subjects diagnosed with Alzheimer's disease, collected from Alzheimer's Disease Neuroimaging Initiative (ADNI)³ dataset, each with structural T1-w MR image. Table 2 displays the data distribution. We used FreeSurfer (Fischl, 2012) to reconstruct both right and left cortical hemispheres for each subject from T1-w MRI. Then we parcellated each cortical hemisphere into 35 cortical regions using Desikan-Killiany Atlas. For each subject k , we defined 4 brain modalities through generating $n_v = 4$ cortical morphological networks as defined in Mahjoub et al. (2018): \mathbf{V}_k^1 denotes the maximum principal curvature brain view, \mathbf{V}_k^2 denotes the mean cortical thickness brain view, \mathbf{V}_k^3 denotes the mean sulcal depth brain view, and \mathbf{V}_k^4 denotes the mean of average curvature as illustrated in Fig. 2. For a given view v , each coefficient $\mathbf{V}_k^v(i, j)$ is defined as the absolute difference between the mean of a view's cortical attribute of the i 'th and the j 'th ROI. For SNF parameters, the number of iterations is set to $N_t = 20$ as it

² http://fcon_1000.projects.nitrc.org/indi/abide/

³ http://adni.loni.usc.edu/wpcontent/uploads/how_to_apply/ADNI

Table 2
Table of evaluation and validation data distribution. M: male, F: female. Total: total number of subjects in each group.

	ASD	NC	AD
M	140	155	23
F	15	31	18
Total	155	186	41
Mean age	16.9	16.6	75.27

guarantees SNF convergence (Wang et al., 2014). We set the number of nearest neighbors to $q = 20$ and for the clustering we used $N_c = 5$ clusters for ASD dataset, $N_c = 6$ for NC dataset and $N_c = 4$ for AD dataset using multi-fold cross-validation.

Evaluation, reproducibility and comparison methods. To evaluate the centeredness of the estimated connectional cortical template, we used two distances: (1) the average distance to the original space between the estimated template and each view of each subject, and (2) the average distance to the mapped space between the estimated template and the fused views of each subject. The metric used for the evaluation is the mean Frobenius distance calculated as: $d_F(A, B) = \sqrt{\sum_i \sum_j |a_{ij} - b_{ij}|^2}$. A smaller distance indicates a more centered network atlas with respect to all individuals in the population and all views. The evaluation of the proposed method in comparison to baseline methods was validated using five randomized partitioning of data samples using five-fold cross-validation, and tested using two populations of right and left hemisphere cortical brain networks: ASD and NC. We compared our proposed cluster-based network fusion (SCA) method to other baseline methods based on the adopted fusion techniques: (1) average-average (AA) method that first averages views for each subject, then averages across subjects, (2) average-SNF (AS) which first linearly averages views for each subject and then non-linearly fuses the obtained views using SNF, (3) the SNF-SNF (SS) technique which uses SNF to first fuse views for each subject, then merges all fused networks across subjects using SNF. Each of these distances is calculated in: (1) the original space (mean distance between the estimated template and the original views V_k^i), and the mapped space (mean distance between the estimated template and the fused views F_k).

As shown in Fig. 3, the proposed method (SCA) gave on average more centered network atlases for both ASD and NC populations in the original space followed by SNF-Average, average-SNF, SNF-SNF and Average-Average methods. Average-average technique produced the highest template-to-population distance for ASD LH {16.22 (average across folds), 16.05 (fold 1), 16.36 (fold 2), 16.42 (fold 3), 16.00 (fold 4), 16.26 (fold 5)}, {16.39 (average across folds), 16.31 (fold 1), 16.44 (fold 2), 16.41 (fold 3), 16.40 (fold 4), 16.38 (fold 5)} for NC LH, {16.11 (average across folds), 16.03 (fold 1), 16.19 (fold 2), 16.38 (fold 3), 16.79 (fold 4), 16.15 (fold 5)} for ASD RH and {16.36 (average across folds), 16.31 (fold 1), 16.41 (fold 2), 16.34 (fold 3), 16.45 (fold 4), 16.29 (fold 5)} for NC RH, respectively. We did not directly include this in Fig. 3 as they fall far away from the distance range of other methods. These results can be explained by the fact that the different views of the brain networks lie on different manifolds, which requires a non-linear fusion technique in order to combine the multiple types of data and bring them into a common space. Therefore, we used the SNF technique in the original space to integrate the multiple views into a single connectivity network for each subject in the population. The obtained fused networks then belong to the mapped space where they become all closer to one another through iterative diffusion (step 2). Hence, we used cluster-based averaging as a linear fusion method to merge fused networks in the mapped space.

Unlike simple averaging which treats all subjects equally in the fusion process, partitioning of the fused views into different clusters and calculating the mean of the clusters' representatives would take into consideration the different patterns (Ecker et al., 2010; Lao et al., 2004; Casanova and Trippe, 2009) in a population by assigning an equal weight to each distribution patterns. Such hierarchical process would solve the problem of inter-variability across subjects offering a well representative template. Therefore, our method (SCA) achieved the best performance in terms of centeredness in the original space especially for ASD population for both hemispheres and across all data partition folds (Fig. 3). Besides, when evaluating the centeredness of the template in the mapped space (Fig. 4), SA remarkably outperformed SS while SCA caused a slight increase in the distance between the estimated template and the fused views. This might indicate that in the mapped space, one might need to use a different clustering method leveraging

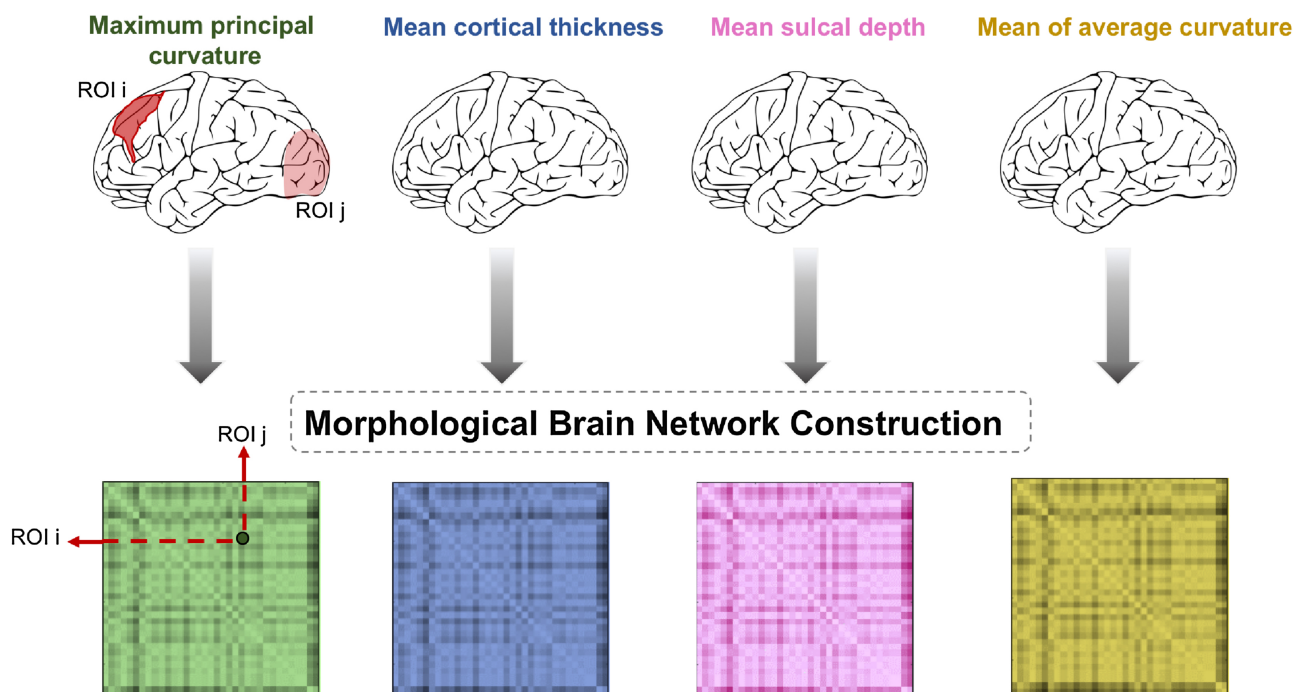


Fig. 2. Morphological brain network construction. Construction of multi-view brain networks using different cortical attributes.

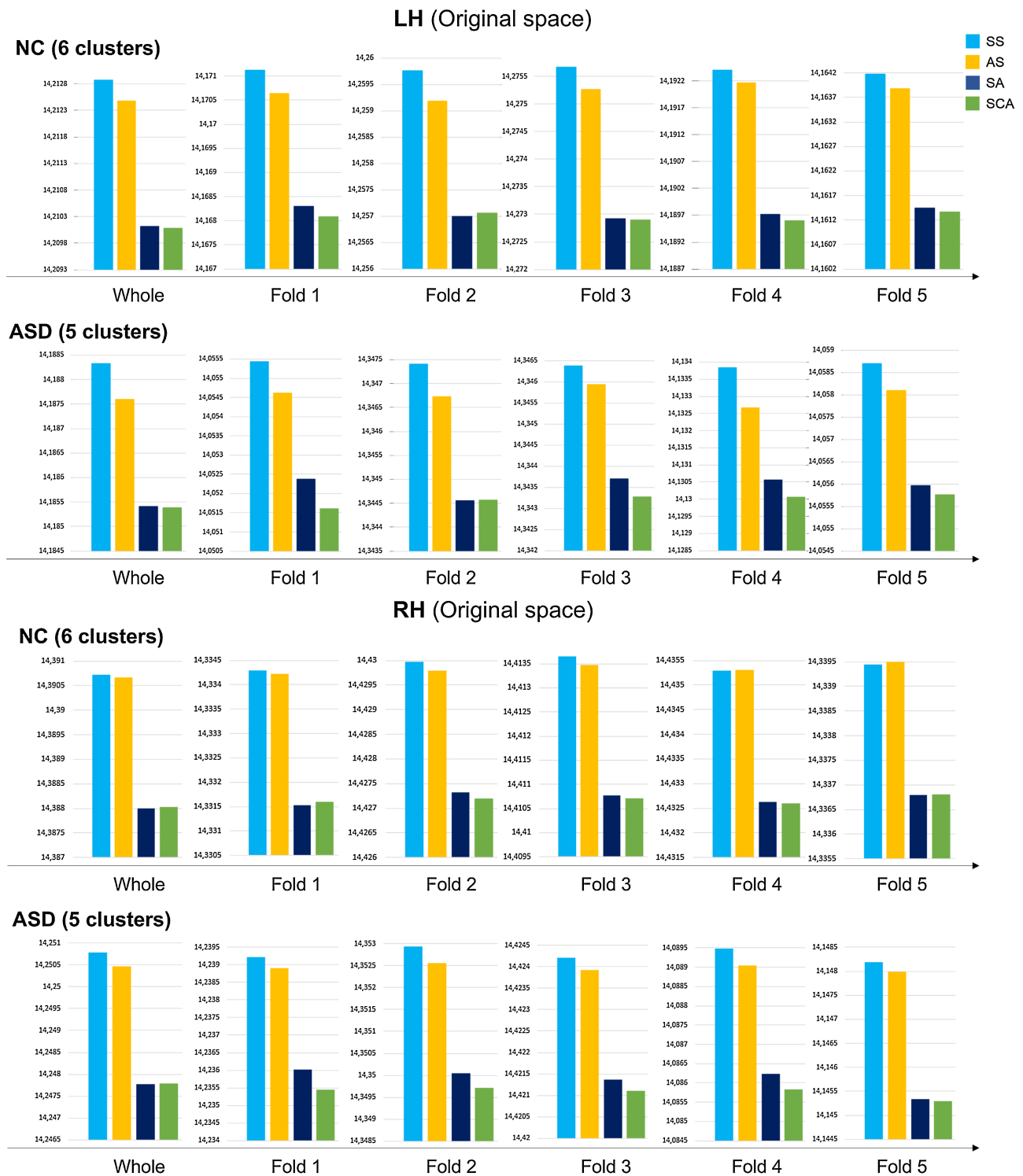


Fig. 3. Evaluation of the morphological multi-view brain network templates estimated for NC and ASD populations using different methods for left (LH) and right (RH) hemispheres. Distance of the estimated templates to views in the original space using SNF-SNF (SS), Average-SNF (AS), SNF-Average (SA) and SNF-Clustering-Average (SCA).

the properties of the fusion space to produce a more centered cluster-based template. The distances in the original space as well as the mapped space are globally consistent for both populations using both hemispheres, yet the differences in results between the right and the left hemispheres for ASD and NC populations can be explained by the fact that both hemispheres present morphological asymmetry (Witelson and Pallie, 1973; Chiron et al., 1995), which generate different templates with different centeredness rates.

Validation on an additional test set. To show the generalizability of our approach to different brain disorders, we evaluated our method and comparison methods on a validation test set composed of 41 subjects diagnosed with Alzheimer's disease for left and right hemispheres independently. As we can see in Fig. 5, overall our method achieved the best performances in the original space followed by SA, AS, SS and AA with the highest distances equal to {14.18 (average across folds), 14.18 (fold 1), 14.12 (fold 2), 14.13 (fold 3), 14.19 (fold 4), 14.28 (fold 5)} for

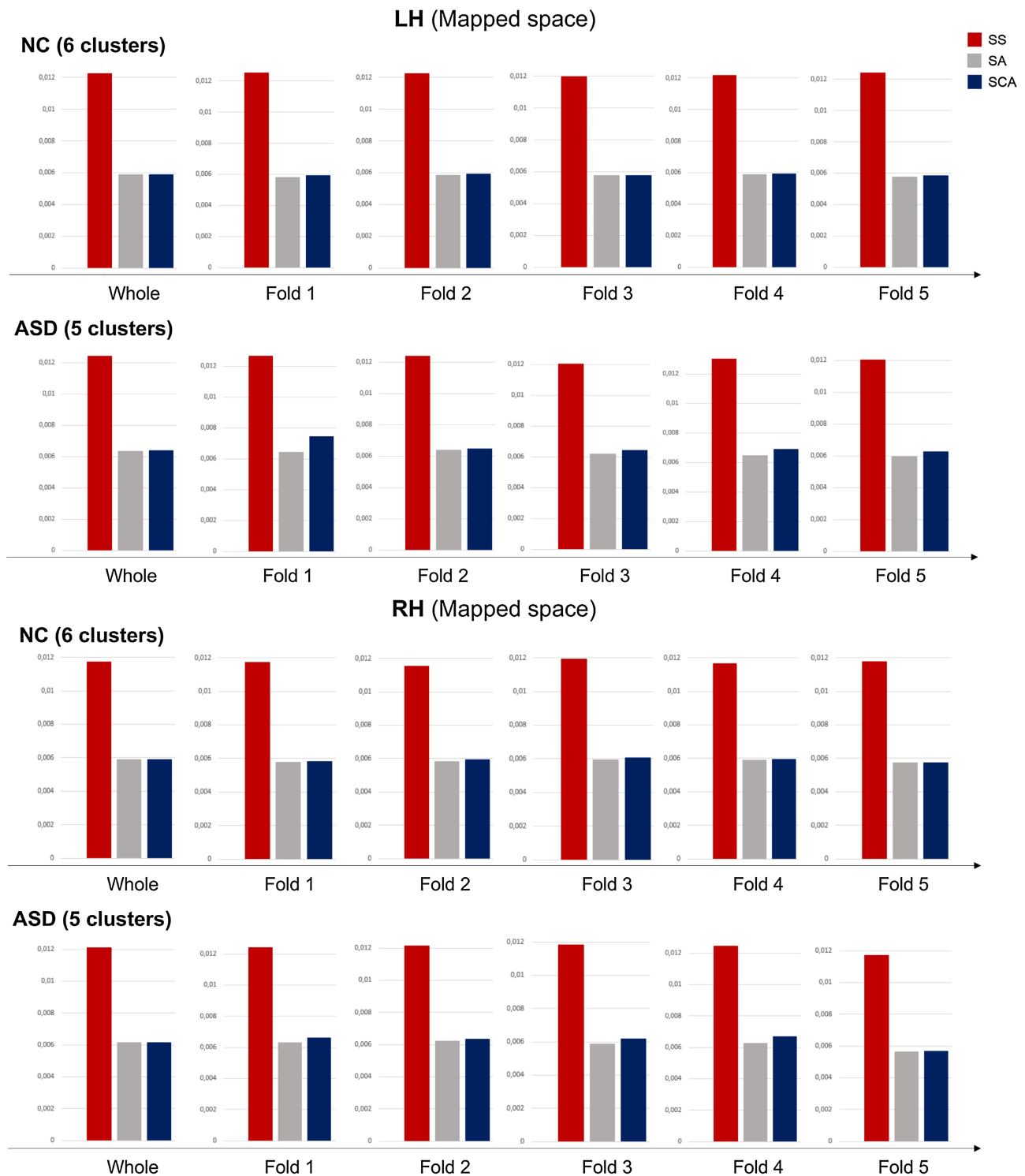


Fig. 4. Evaluation of the morphological multi-view brain network templates estimated for NC and ASD populations using different methods for left (LH) and right (RH) hemispheres. Distance to views in the mapped space of the estimated atlases using SNF-SNF (SS), SNF-Average (SA) and SNF-Clustering-Average (SCA).

AD LH and {14.26 (average across folds), 14.22 (fold 1), 14.20 (fold 2), 14.29 (fold 3), 14.28 (fold 4), 14.30 (fold 5)} for AD RH, respectively. Fig. 5 shows consistent results for the validation dataset (AD population) in comparison with the evaluation datasets (ASD and NC populations) in both the original and the mapped spaces.

Insights into discriminative multi-view connective features. To investigate multi-view morphological connective differences between autistic and healthy subjects, we identified the top 5 discriminative connections for each hemisphere distinguishing between

both groups using the estimated morphological brain templates as shown in Fig. 6. For each hemisphere, by computing the absolute difference between the healthy and disordered template, we identified the top ROIs with the highest distance values. We believe that the difference between top discriminative regions in the right and left hemispheres are due to the asymmetric nature of the human brain (Witelson and Pallie, 1973; Wada et al., 1975) as well as the asymmetric influence of autism on the morphological aspects between both hemispheres (Chiron et al., 1995; Herbert et al., 2004, 2002). Several identified

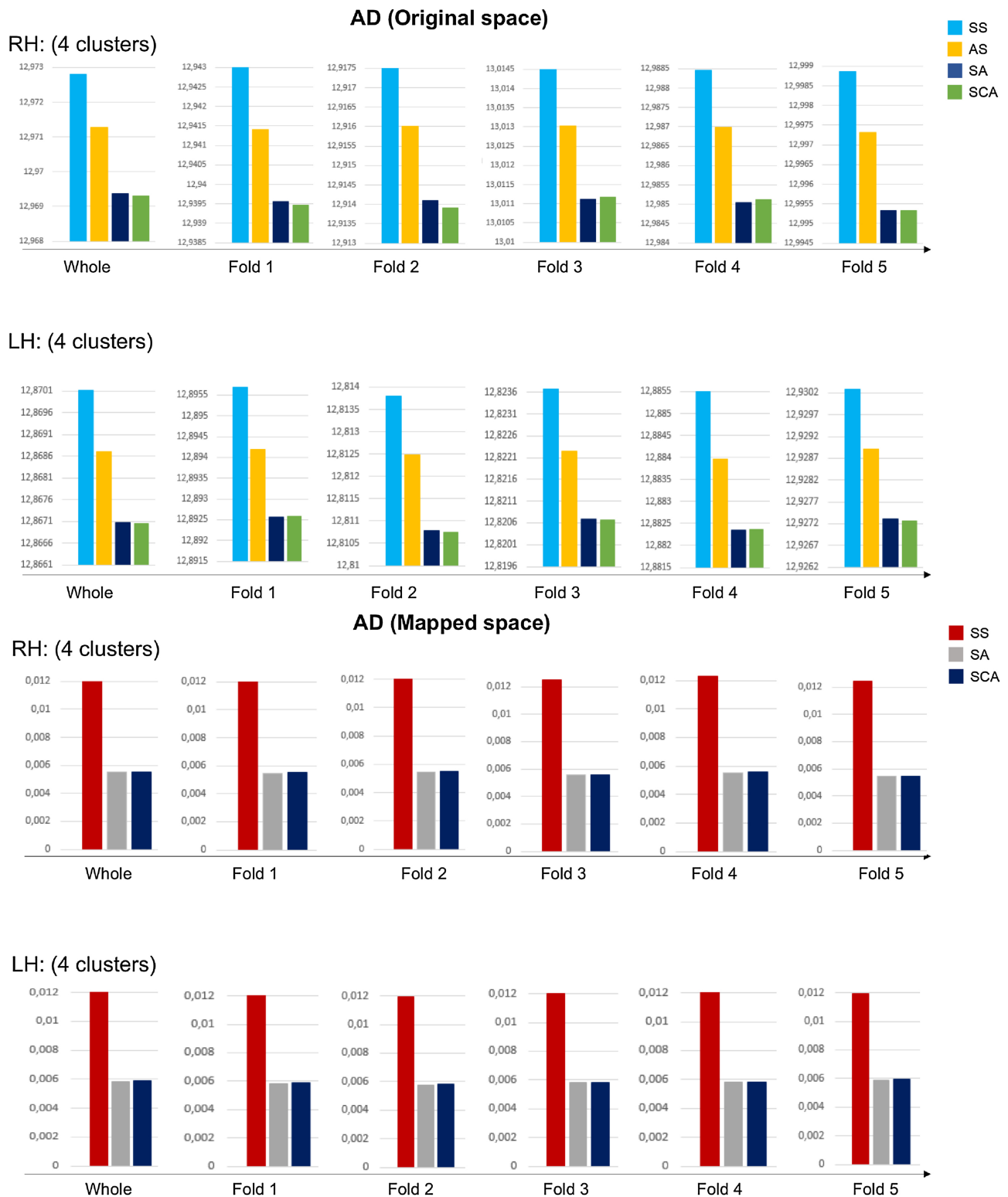


Fig. 5. Evaluation of the morphological multi-view brain network templates estimated for AD population using different methods for left (LH) and right (RH) hemispheres. Distance to views in both the original and the mapped space of the estimated atlases using SNF-SNF (SS), SNF-Average (SA) and SNF-Clustering-Average (SCA).

discriminative cortical ROIs were consistent with previous ASD studies in the literature (Doyle-Thomas et al., 2013; Amaral et al., 2008; Just et al., 2006; Blatt, 2012; Wegiel et al., 2010) such as the anterior-cingulate cortex, which is responsible for the repetitive behavior in autistic subjects, the inferior parietal cortex leading to attentional deficits and the posterior cingulate cortex, as well as the left isthmus cingulate cortex, the right insula and the medial orbital frontal cortex,

responsible for the social impairment related to autism.

Several ROIs were identified in more than a single discriminative connection such as the left and the right lingual gyri, which were present in the 3rd and 5th, and the 2nd and 4th discriminative connections, respectively. A recent study (Zielinski et al., 2014) conducted to investigate the abnormality of cortical morphological changes in autistic subjects over time has shown that both left and right lingual

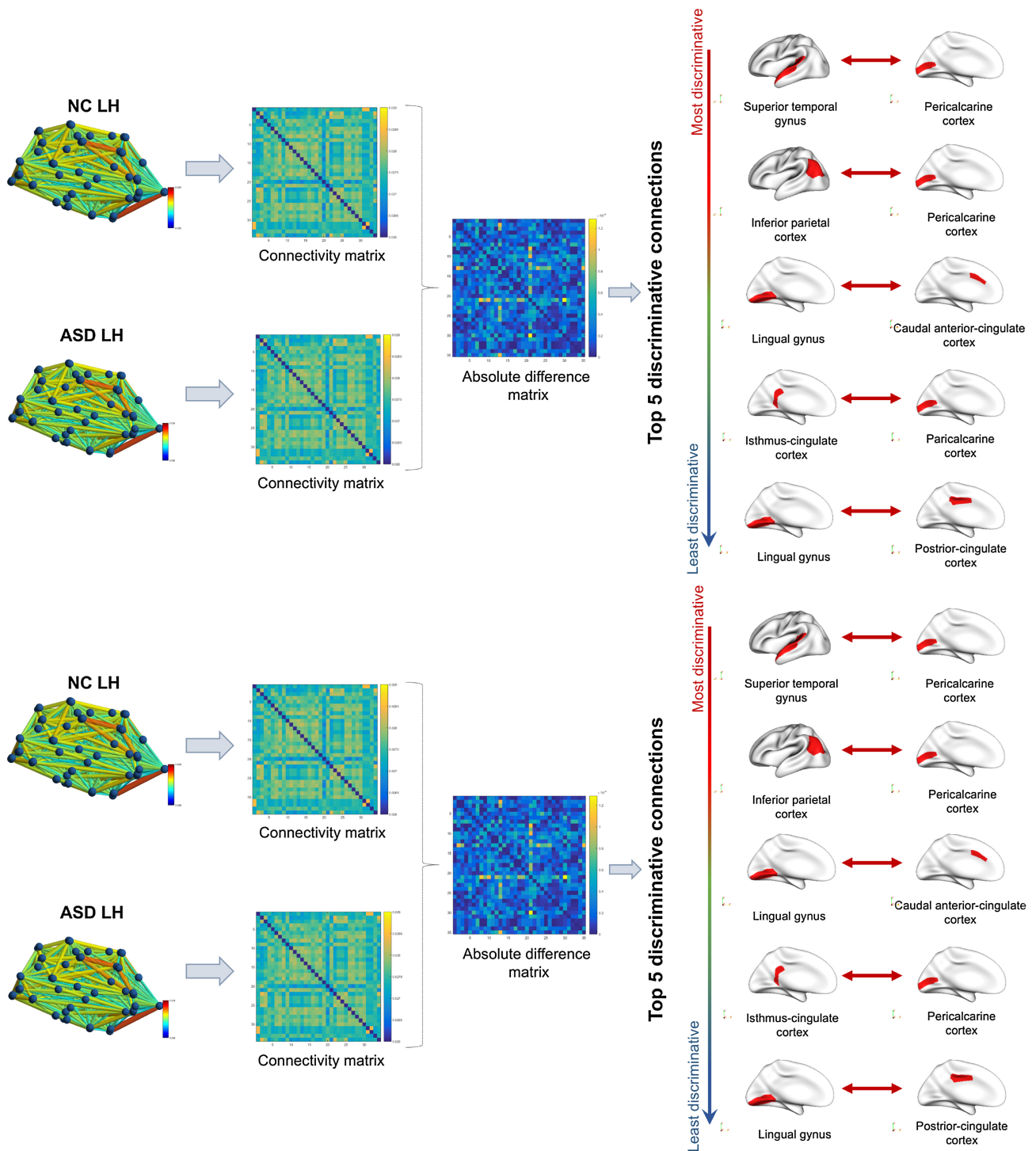


Fig. 6. Comparison between NC and ASD multi-view network atlases and identification of top 5 discriminative connections between both templates for the left (top) and right (bottom) hemispheres.

gyri had different morphological development compared to normal subjects. In fact, the left lingual gyrus was thicker during childhood in autistic subjects while the right lingual gyrus was thinner by adulthood. The same study has shown a decrease in the parahippocampal thickness in ASD, a cortical ROI that was found in the 1st and 3rd discriminative connections in the right hemisphere using our estimated templates. Pericalcarine cortex, on the other hand, was identified in the 1st, 2nd and 4th discriminative connections in the left hemisphere. Cortical changes in this region of the brain were related to autism in the

childhood with high statistical significance (p -value < 0.01) as reported in Zielinski et al. (2014).

In summary, the proposed method had the best results in terms of centeredness in the original space compared to other baseline methods, yet it fell behind the proposed SA in terms of centeredness in the mapped space. We note that our proposed framework is generalizable to different modalities or views and different parcellation templates under the condition that we keep a consistent parcellation across all modalities and across all subjects. In our future work, we will further

refine this framework through leveraging manifold learning techniques to generate centered network atlases in both original and mapped spaces. In addition, we will build brain network atlases for healthy individuals as well as patients with other brain disorders (e.g., dementia) to better identify population-based distinctive changes in brain connectivity, thereby providing reliable features or biomarkers for an accurate diagnosis. Last, building a multi-view brain network atlas that integrates morphological, functional and structural brain networks in a single reference template might help reveal how brain morphology relates to brain function and structure. Our cortical brain network atlases can also be integrated with the recently introduced brain kinectomes (i.e., population-based brain growth templates) Rezik et al. (2018a, 2018b), to investigate the connective relationship between brain morphology and kinetics in health and disease.

4. Conclusion

In this work, we unprecedentedly proposed a population-based multi-view network fusion framework for estimating a multi-view brain network atlas for both healthy and disordered populations. Our method had the best results in terms of centeredness when tested on morphological brain networks, yet it can be applied to all types of brain networks (e.g., structural or function). Building multimodal brain network atlases can be utilized as ‘references’ to normalize individual brain networks for comparative studies. In our future work, we will explore multi-manifold learning methods for nesting brain views, which will eventually produce more robust clustering results to outliers in both original and mapped spaces.

Acknowledgements

Data collection and sharing for this project was funded by the Alzheimer's Disease Neuroimaging Initiative (ADNI) (National Institutes of Health Grant U01 AG024904) and DOD ADNI (Department of Defense award number W81XWH-12-2-0012). ADNI is funded by the National Institute on Aging, the National Institute of Biomedical Imaging and Bioengineering, and through generous contributions from the following: AbbVie, Alzheimer's Association; Alzheimer's Drug Discovery Foundation; Araclon Biotech; BioClinica, Inc.; Biogen; Bristol-Myers Squibb Company; CereSpir, Inc.; Cogstate; Eisai Inc.; Elan Pharmaceuticals, Inc.; Eli Lilly and Company; EuroImmun; F. Hoffmann-La Roche Ltd and its affiliated company Genentech, Inc.; Fujirebio; GE Healthcare; IXICO Ltd.; Janssen Alzheimer Immunotherapy Research & Development, LLC.; Johnson & Johnson Pharmaceutical Research & Development LLC.; Lumosity; Lundbeck; Merck & Co., Inc.; Meso Scale Diagnostics, LLC.; NeuroRx Research; Neurotrack Technologies; Novartis Pharmaceuticals Corporation; Pfizer Inc.; Piramal Imaging; Servier; Takeda Pharmaceutical Company; and Transition Therapeutics. The Canadian Institutes of Health Research is providing funds to support ADNI clinical sites in Canada. Private sector contributions are facilitated by the Foundation for the National Institutes of Health (www.fnih.org). The grantee organization is the Northern California Institute for Research and Education, and the study is coordinated by the Alzheimer's Therapeutic Research Institute at the University of Southern California. ADNI data are disseminated by the Laboratory for Neuro Imaging at the University of Southern California.

References

Amaral, D.G., Schumann, C.M., Nordahl, C.W., 2008. Neuroanatomy of autism. *Trends Neurosci.* 31, 137–145.
 Blatt, G.J., 2012. The neuropathology of autism. *Scientifica* 2012.
 Bosc, M., Heitz, F., Armspach, J.P., Namer, I., Gounot, D., Rumbach, L., 2003. Automatic change detection in multimodal serial MRI: application to multiple sclerosis lesion evolution. *NeuroImage* 20, 643–656.
 Brown, C., Hamarneh, G., 2016. Machine learning on human connectome data from MRI. [arXiv:1611.08699v1](https://arxiv.org/abs/1611.08699v1).

Bullmore, E., Bassett, D., 2011. *Brain Graphs* 7, 113–140.
 Bullmore, E., Sporns, O., 2009. Complex brain networks: graph theoretical analysis of structural and functional systems. *Nat. Neurosci.* 10, 186–198.
 Calhoun, V.D., Sui, J., 2016. Multimodal fusion of brain imaging data: A key to finding the missing link (s) in complex mental illness. *Biol. Psychiatry: Cognit. Neurosci. Neuroimaging* 1, 230–244.
 Casanova, M., Trippe, J., 2009. Radial cytoarchitecture and patterns of cortical connectivity in autism. *Philos. Trans. R. Soc. B: Biol. Sci.* 364, 1433–1436.
 Chiron, C., Leboyer, M., Leon, F., Jambaque, L., Nuttin, C., Syrota, A., 1995. Spect of the brain in childhood autism: evidence for a lack of normal hemispheric asymmetry. *Develop. Med. Child Neurol.* 37, 849–860.
 Doyle-Thomas, K.A., Kushki, A., Duerden, E.G., Taylor, M.J., Lerch, J.P., Soorya, L.V., Wang, A.T., Fan, J., Anagnostou, E., 2013. The effect of diagnosis, age, and symptom severity on cortical surface area in the cingulate cortex and insula in autism spectrum disorders. *J. Child Neurol.* 28, 732–739.
 Ecker, C., Marquand, A., Mour ao-Miranda, J., Johnston, P., Daly, E.M., Brammer, M.J., Maltezos, S., Murphy, C.M., Robertson, M., Williams, S.C., et al., 2010. Describing the brain in autism in five dimensions-magnetic resonance imaging-assisted diagnosis of autism spectrum disorder using a multiparameter classification approach. *J. Neurosci.* 30, 10612–10623.
 Fischl, B., 2012. *Freerunner. Neuroimage* 62, 774–781.
 Herbert, M.R., Harris, G.J., Adrien, K.T., Ziegler, D.A., Makris, N., Kennedy, D.N., Lange, N.T., Chabris, C.F., Bakardjiev, A., Hodgson, J., et al., 2002. Abnormal asymmetry in language association cortex in autism. *Ann. Neurol.* 52, 588–596.
 Herbert, M.R., Ziegler, D.A., Deutsch, C., O'Brien, L.M., Kennedy, D.N., Filipek, P., Bakardjiev, A., Hodgson, J., Takeoka, M., Makris, N., et al., 2004. Brain asymmetries in autism and developmental language disorder: a nested whole-brain analysis. *Brain* 128, 213–226.
 Hinrichs, C., Singh, V., Xu, G., Johnson, S.C., Initiative, A.D.N., et al., 2011. Predictive markers for ad in a multi-modality framework: an analysis of mci progression in the adni population. *Neuroimage* 55, 574–589.
 Holmes, A.J., Hollinshead, M.O., O'Keefe, T.M., Petrov, V.I., Fariello, G.R., Wald, L.L., Fischl, B., Rosen, B.R., Mair, R.W., Roffman, J.L., et al., 2015. Brain genomics superstruct project initial data release with structural, functional, and behavioral measures. *Sci. Data* 2, 150031.
 Iftekharuddin, K.M., Zheng, J., Islam, M.A., Ogg, R.J., 2009. Fractal-based brain tumor detection in multimodal MRI. *Appl. Math. Comput.* 207, 23–41.
 Just, M.A., Cherkassky, V.L., Keller, T.A., Kana, R.K., Minshew, N.J., 2006. Functional and anatomical cortical underconnectivity in autism: evidence from an fmri study of an executive function task and corpus callosum morphometry. *Cerebral Cortex* 17, 951–961.
 Lao, Z., Shen, D., Xue, Z., Karacali, B., Resnick, S.M., Davatzikos, C., 2004. Morphological classification of brains via high-dimensional shape transformations and machine learning methods. *Neuroimage* 21, 46–57.
 Lerch, J.P., van der Kouwe, A.J., Raznahan, A., Paus, T., Johansen-Berg, H., Miller, K.L., Smith, S.M., Fischl, B., Sotiropoulos, S.N., 2017. Studying neuroanatomy using mri. *Nat. Neurosci.* 20, 314.
 Lisowska, A., Rezik, I., Initiative, A.D.N., et al., 2017. Pairing-based ensemble classifier learning using convolutional brain multiplexes and multi-view brain networks for early dementia diagnosis. *International Workshop on Connectomics in Neuroimaging* 42–50.
 Mahjoub, I., Mahjoub, M.A., Rezik, I., 2018. Brain multiplexes reveal morphological connective biomarkers fingerprinting late brain dementia states. *Sci. Rep.* 8, 4103.
 Rezik, I., Li, G., Lin, W., Shen, D., 2017. Estimation of brain network atlases using diffusive-shrinking graphs: Application to developing brains. *International Conference on Information Processing in Medical Imaging* 385–397.
 Rezik, I., Li, G., Lin, W., Shen, D., 2018a. Do baby brain cortices that look alike at birth grow alike during the first year of postnatal development? *MICCAI*.
 Rezik, I., Li, G., Lin, W., Shen, D., 2018b. Estimation of shape and growth brain network atlases for connectomic brain mapping in developing infants. *Medical Image Computing and Computer-Assisted Intervention-MICCAI*.
 Soussia, M., Rezik, I., 2017. High-order connectomic manifold learning for autistic brain state identification. *Int. Workshop Connect. Neuroimaging* 51–59.
 Sporns, O., 2012. The human connectome: A complex network. *Schizophrenia Res.* 136, S28.
 Sporns, O., 2013. The human connectome: origins and challenges. *Neuroimage* 80, 53–61.
 Sui, J., Adali, T., Yu, Q., Chen, J., Calhoun, V.D., 2012. A review of multivariate methods for multimodal fusion of brain imaging data. *J. Neurosci. Methods* 204, 68–81.
 Thung, K.H., Wee, C.Y., Yap, P.T., Shen, D., Initiative, A.D.N., et al., 2014. Neurodegenerative disease diagnosis using incomplete multi-modality data via matrix shrinkage and completion. *NeuroImage* 91, 386–400.
 Tong, T., Gray, K., Gao, Q., Chen, L., Rueckert, D., 2015. *Nonlinear Graph Fusion for Multi-modal Classification of Alzheimer's Disease*. Springer, pp. 77–84.
 Uludağ, K., Roebroeck, A., 2014. General overview on the merits of multimodal neuroimaging data fusion. *Neuroimage* 102, 3–10.
 Uylings, H., Rajkowska, G., Sanz-Arigitia, E., Amunts, K., Zilles, K., 2005. Consequences of large interindividual variability for human brain atlases: converging macroscopic imaging and microscopical neuroanatomy. *Anatomy Embryol.* 210, 423–431.
 Van Essen, D.C., Glasser, M.F., 2016. The human connectome project: Progress and prospects. *Cerebrum* 2016.
 Van Essen, D.C., Smith, S.M., Barch, D.M., Behrens, T.E., Yacoub, E., Ugurbil, K., Consortium, W.M.H., et al., 2013. The WU-Minn human connectome project: an overview. *Neuroimage* 80, 62–79.
 Van Essen, D.C., Ugurbil, K., Auerbach, E., Barch, D., Behrens, T., Bucholz, R., Chang, A., Chen, L., Corbetta, M., Curtiss, S.W., et al., 2012. The Human Connectome Project: a

- data acquisition perspective. *Neuroimage* 62, 2222–2231.
- Wada, J.A., Clarke, R., Hamm, A., 1975. Cerebral hemispheric asymmetry in humans: Cortical speech zones in 100 adult and 100 infant brains. *Arch. Neurol.* 32, 239–246.
- Wang, B., Mezlini, A., Demir, F., Fiume, M., et al., 2014. Similarity network fusion for aggregating data types on a genomic scale. *Nat. Methods* 11, 333–337.
- Wee, C.Y., Yap, P.T., Zhang, D., Denny, K., Brownndyke, J.N., Potter, G.G., Welsh-Bohmer, K.A., Wang, L., Shen, D., 2012. Identification of mci individuals using structural and functional connectivity networks. *Neuroimage* 59, 2045–2056.
- Wegiel, J., Kuchna, I., Nowicki, K., Imaki, H., Wegiel, J., Marchi, E., Ma, S.Y., Chauhan, A., Chauhan, V., Bobrowicz, T.W., et al., 2010. The neuropathology of autism: defects of neurogenesis and neuronal migration, and dysplastic changes. *Acta Neuropathol.* 119, 755–770.
- Witelson, S.F., Pallie, W., 1973. Left hemisphere specialization for language in the newborn: Neuroanatomical evidence of asymmetry. *Brain* 96, 641–646.
- Yuan, L., Wang, Y., Thompson, P.M., Narayan, V.A., Ye, J., Initiative, A.D.N., et al., 2012. Multi-source feature learning for joint analysis of incomplete multiple heterogeneous neuroimaging data. *NeuroImage* 61, 622–632.
- Zhang, D., Wang, Y., Zhou, L., Yuan, H., Shen, D., Initiative, A.D.N., et al., 2011. Multimodal classification of alzheimer's disease and mild cognitive impairment. *Neuroimage* 55, 856–867.
- Zielinski, B.A., Prigge, M.B., Nielsen, J.A., Froehlich, A.L., Abildskov, T.J., Anderson, J.S., Fletcher, P.T., Zygumunt, K.M., Travers, B.G., Lange, N., et al., 2014. Longitudinal changes in cortical thickness in autism and typical development. *Brain* 137, 1799–1812.